AIAA JOURNAL
Vol. 40, No. 5, May 2002

Drag Reduction by Spanwise Wall Oscillation in Wall-Bounded Turbulent Flows

Jung-Il Choi*
Korea Advanced Institute of Science and Technology, Taejon 305-701, Republic of Korea
Chun-Xiao Xu†
Tsinghua University, Beijing 100084, People's Republic of China
and
Hyung Jin Sung‡
Korea Advanced Institute of Science and Technology, Taejon 305-701, Republic of Korea

Drag reduction in turbulent channel and pipe flows by spanwise (circumferential) wall oscillations is studied numerically. The influence of the wall oscillation on near-wall streamwise vortices is examined. By the use of the Stokes second problem, a wall-normal distance parameter and an acceleration parameter are obtained to estimate the drag reduction rate. A simple equation is derived for expressing the drag reduction rate by spanwise wall oscillations. The relation between near-wall streamwise vortices and low- and high-speed fluids is scrutinized to extract the key parameters. The drag reduction mechanism is analyzed in terms of the attenuation of Reynolds shear stress.

Nomenclature

A^+	=	oscillating velocity amplitude of the wall
a^+	=	acceleration of the Stokes layer
D_r	=	drag reduction rate
h	=	channel half width
Q	=	invariant of the velocity gradient tensor
S_{ij}	=	the tensor of strain rate
T^+	=	oscillating time period of the wall
t^+	=	nondimensional time, tu_τ^2/ν
u_τ	=	friction velocity
W	=	mean spanwise velocity
W^+	=	nondimensional mean spanwise velocity, W/u_τ
W^+_{env}	=	nondimensional envelope of W^+
y^+	=	nondimensional wall-normal distance, yu_τ/ν
y^+_d	=	influence range of the Stokes layer
ν	=	kinematic viscosity
Ω_{ij}	=	tensor of rotation
ω_x	=	streamwise voritcity

Introduction

THE role of near-wall streamwise vortices has been found to be very important in a wall-bounded turbulent flow.[1] The downward sweep motion induced by streamwise vortices very near the wall is closely correlated with skin friction.[2] Consequently, to achieve a reduction of skin friction, the management of near-wall streamwise vortices has been a target of control strategies. A recently devised method for drag reduction in wall-bounded turbulent flows is a cyclic movement of the wall in the spanwise (circumferential) direction. When the wall oscillation is optimized with appropriate amplitude and frequency, a significant drag reduction is achieved by as much as 40%. Although energy is needed for the motion of the wall, no feedback is required in the control law.

A literature survey reveals that many experimental and numerical studies have been performed to examine the drag reduction by spanwise oscillations. Jung et al.[3] showed numerically the suppression of turbulence in wall-bounded turbulent channel flows by high-frequency spanwise oscillations. Laadhari et al.[4] and Choi et al.[5] carried out an experimental study in a turbulent boundary layer to confirm the numerical results experimentally. The effects of wall-oscillation amplitude on the total energy balance was investigated by Baron and Quadrio[6] using a direct numerical simulation. An experimental study of turbulent pipe flows was performed by Choi and Graham[7] with a view to reduce the friction drag by oscillating a section of the pipe in a circumferential direction. The results indicated that the friction factor is reduced by as much as 25% as a result of active manipulation of near-wall turbulence structures by circumferential wall oscillation. The mechanism of drag reduction may be related to the spanwise vorticity generated by the periodic Stokes layer over the oscillating wall, which affects the boundary-layer profile by reducing the mean velocity gradient within the viscous sublayer.[5,7] Recently, Quadrio and Sibilla[8] performed direct numerical simulations in a pipe oscillating around its axis. They found that the transverse shear layer arising from the oscillations induces substantial modifications to the turbulence statistics in the near-wall region.

A perusal of the literature indicates that many parametric studies have been performed to find the best parameters in terms of friction drag reduction. The frequency and amplitude of the oscillations obviously play a first-order role in determining the amount of the turbulent drag reduction rate. The choice of the optimum parameters, however, still has to be determined. The main aim of this work is to find the optimum parameters. This is clearly related to the Stokes layer, which is generated by the oscillating wall. The approach is to use the solution to the Stokes second problem to obtain estimates of how far from the wall the influence of oscillations extends and of the acceleration that they produce very near the wall. Toward this end, direct numerical simulations in channel and pipe flows are performed to obtain detailed results for the turbulent flow behavior near the wall and to correlate that behavior in terms of a wall-normal distance parameter and an acceleration parameter based on the Stokes solution. Emphasis is placed on the identification of the relation between the near-wall streamwise vortices and low- and high-speed fluids by spanwise oscillations. The mechanism of drag reduction is analyzed in terms of the Reynolds shear stress.

Received 14 August 2001; revision received 27 November 2001; accepted for publication 3 December 2001.

*Ph.D. Student, Department of Mechanical Engineering, 373-1, Kusong-dong, Yusong-gu.
†Assistant Professor, Department of Engineering Mechanics.
‡Professor, Department of Mechanical Engineering, 373-1, Kusong-dong, Yusong-gu; hsung@kaist.ac.kr. Member AIAA.

Second Stokes Problem

We start with the notion that the key to drag reduction is to disturb the wall-bounded flow between the near-wall streamwise vortices and the wall. When a temporal wall oscillation is imposed, the governing equation for the mean spanwise velocity, ignoring the higher-order nonlinear terms, can be expressed as[9]

$$\frac{\partial W^+}{\partial t^+} = \frac{\partial^2 W^+}{\partial y^{+2}} \tag{1}$$

subject to

$$W^+(y^+ = 0, t^+) = A^+ \sin(2\pi t^+/T^+) \tag{2}$$

$$W^+(y^+ \to \infty, t^+) = 0 \tag{3}$$

Here, the nondimensional parameters are $W^+ = W/u_\tau$, $A^+ = A/u_\tau$, $y^+ = yu_\tau/\nu$, $t^+ = tu_\tau^2/\nu$, and $T^+ = Tu_\tau^2/\nu$; u_τ is the wall friction velocity for flows with a stationary wall and ν is the kinematic viscosity of the fluid. The flow quantities are normalized by wall units u_τ and ν. The nondimensional envelope of the real part of the solution for $W^+(y^+, t^+)$ at a certain location y^+ is

$$W^+_{\text{env}} = A^+ \exp\left[-\sqrt{(\pi/T^+)}y^+\right] \tag{4}$$

In the preceding description, the wall oscillation decays exponentially far from the wall. It is found that Eq. (1) is similar to the Stokes second problem.[10]

To see the response of near-wall turbulence to spanwise wall oscillations, the instantaneous spanwise mean velocity profiles by the present simulation are displayed in Fig. 1a. The Reynolds number is $Re_m = 4.9 \times 10^3$ ($Re_\tau = 1.7 \times 10^2$), which is based on the bulk mean velocity U_m and pipe diameter D for $A^+ = 0.8U_m$ and $T^+ = 150$. The different curves in Fig. 1 represent different instances in time during the oscillating period. The analytical solutions at the same oscillating conditions are also shown in Fig. 1b, which are obtained from Eq. (4). The two plots are very similar to each other. This supports that the near-wall structures are dominated by the spanwise oscillating parameters A^+ and T^+.

Direct Numerical Simulations

As mentioned earlier, direct numerical simulations of turbulent channel and pipe flows with oscillating walls are performed in the present study. The numerical method for solving the Navier–Stokes equations in a turbulent channel flow is based on a semi-implicit method.[2] Both a Chebyshev-tau method in the wall normal direction and a dealiased Fourier method in the streamwise and spanwise directions are used for the spatial derivatives. A semi-implicit time advancement scheme is employed by using the Crank–Nicolson implicit method for the viscous terms and an explicit third-order Runge–Kutta scheme for the nonlinear terms. The spectral numerical scheme used in this study is nearly the same as that used by Kim et al.[2] Three Reynolds number flows are tested: $Re_\tau = 100, 200$, and 400. The domain sizes for three Reynolds number flows in the streamwise, wall-normal, and spanwise directions are $4\pi h \times 2h \times 4\pi h/3$, $2\pi h \times 2h \times 4\pi h/3$, and $\pi h \times 2h \times \pi h/3$, respectively. Here, h denotes the half-channel width. The grid sizes are $32 \times 65 \times 32$, $64 \times 65 \times 64$, and $64 \times 129 \times 64$, respectively. The code validation has been made by comparing the present data with the preexisting direct numerical simulation (DNS) data. The predicted profiles at $Re_\tau = 180$ have been compared with the data of Kim et al.[2] The grid resolution of the present simulation is $128 \times 129 \times 128$ in the streamwise, wall-normal, and spanwise directions, respectively. The domain size is $4\pi h \times 2h \times 4\pi h/3$. It is found that the present data follow their data very well.

Next, the numerical scheme for simulating a turbulent pipe flow is almost the same as that used by Ma et al.[10] The numerical method is based on the third-order time-splitting method.[11] In the axial and circumferential directions, a Fourier–Galerkin method is employed. In the radial direction, a spectral element method is adopted to avoid the computational unsteadiness caused by the over-fine grids near the center of the pipe. The Reynolds number is $Re_\tau = 150$ and the computational length of the pipe is $4\pi R$. The spatial resolution is $53 \times 64 \times 32$ in the radial, circumferential, and streamwise directions, respectively.

All of the simulations are performed with constant streamwise mass flux. Because the no-slip conditions are satisfied at the wall, the wall oscillations in the spanwise (circumferential) direction are directly taken into account via the wall boundary conditions for the corresponding velocity components. The flow quantities are normalized by the bulk mean velocity U_m and h (or R) except those with the superscript +, which are normalized by wall units u_τ and ν. In the present study, the velocity amplitude of wall oscillation A^+ varies from 1 to 20, and the oscillation period T^+ is set in the range from 1 to 200 for turbulent channel flow and turbulent pipe flow.

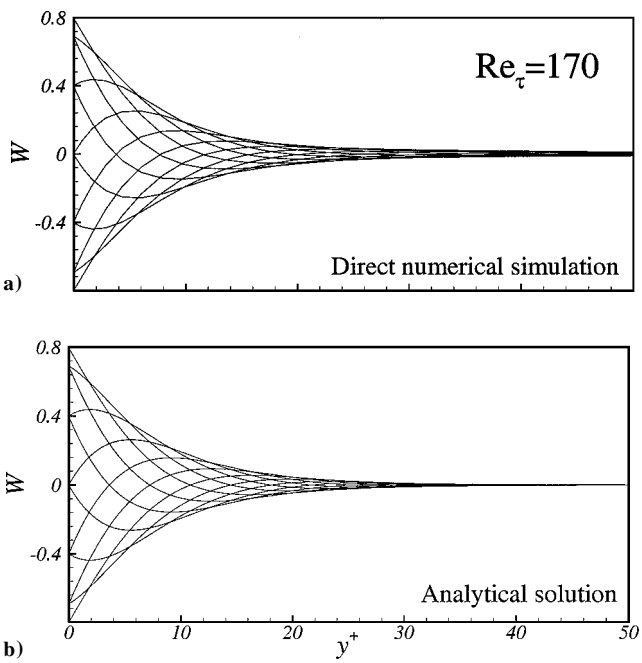

Fig. 1 Mean spanwise velocity profiles; different curves represent different instances in time during an oscillating period.

Results and Discussion

The first objective of the present simulation is to estimate a simple equation expressing the friction drag reduction by spanwise oscillations as a primary function of the oscillating parameters. The percentage of drag reduction rate is defined as $D_r(\%) = (\tau_{\text{no}} - \tau_c)/\tau_{\text{no}} \times 100$, where τ_{no} denotes the shear stress without oscillation and τ_c that with spanwise oscillations. As mentioned earlier, several other published numerical and experimental data are employed for comparison: a numerical simulation in turbulent channel flow by Baron and Quadrio,[6] an experimental work in turbulent pipe flow by Choi and Graham,[7] and a numerical simulation in turbulent pipe flow by Quadrio and Sibilla.[8] Details regarding the oscillating conditions are available in the references. The present numerical data are also included: One is from the turbulent channel flow simulations ($Re_\tau = 100$, 200, and 400), and the other is from the turbulent pipe flow simulation ($Re_\tau = 150$). The oscillating conditions of the simulations and the drag reduction results are summarized in Table 1. In Table 1, RLM denotes the relaminarization by circumferential oscillations.

As stated, all of the available data are replotted on D_r by the use of several key parameters. First, D_r is plotted as a function of the oscillating velocity amplitude A^+ in Fig. 2a, where A^+ is the oscillating velocity amplitude of the wall in Eq. (4). Examination of the distributions between D_r and A^+ in Fig. 2a indicates that D_r increases with increasing A^+. However, D_r is not linear against A^+ in some cases. Note that the increase of A^+ means the increase of the extra input of energy by spanwise oscillations. Next, D_r is replotted as a function of the oscillating period T^+ in Fig. 2b. Each line represents different A^+. As T^+ increases, a peak value is seen at around $T^+ \sim 100$. This

Table 1 Drag reduction rate D_r with different A^+ and T^+

	T^+							
A^+	1	5	10	20	50	100	150	200
				Turbulent channel flow ($Re_\tau = 100$)				
1	−0.5	0.3	0.6	1.0	2.6	1.9	1.7	1.6
5	0.6	0.9	3.2	9.8	21.9	29.6	23.6	15.1
10	0.4	2.7	9.7	20.2	33.2	41.1	42.8	33.2
20	−2.0	8.6	19.3	29.6	40.3	44.5	45.4	45.3
				Turbulent channel flow ($Re_\tau = 200$)				
5	——	——	——	——	13.1	18.4	13.6	10.1
10	——	——	——	——	25.7	29.9	26.1	17.4
20	——	——	——	——	34.2	39.2	35.6	21.0
				Turbulent channel flow ($Re_\tau = 400$)				
5	——	——	——	——	9.4	14.2	9.2	7.4
10	——	——	——	——	22.8	22.4	18.3	12.3
20	——	——	——	——	30.6	34.1	25.5	14.2
				Turbulent pipe flow ($Re_\tau = 150$)				
5	——	1.4	2.4	7.9	18.8	22.9	18.8	15.8
10	——	2.0	6.5	17.3	30.6	34.9	RLM[a]	RLM
20	——	8.6	15.7	26.8	39.0	RLM	RLM	RLM

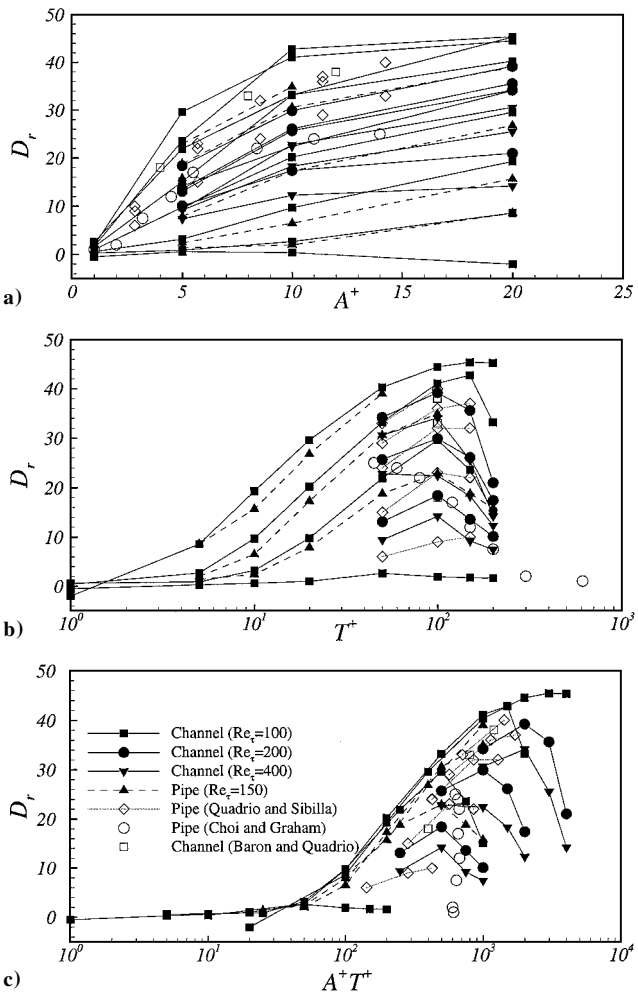

Fig. 2 Drag reduction rate as a function of a) A^+, b) T^+, and c) A^+T^+.

means that a maximum drag reduction is obtained at $T^+ \sim 100$. In Fig. 2c, D_r is plotted as a function of A^+T^+, where the variable A^+T^+ indicates a displacement of the oscillating wall. The maximum displacement is A^+T^+/π. For example, the maximum displacement of the wall of the present channel and pipe flows is about 50 ($A^+T^+/\pi \simeq 50$) at $A^+T^+ = 150$, which represents the mean spacing between low- and high-speed streaks.[12] As seen in Fig. 2c, a better similarity is attained. However, some exceptional cases still remain. A closer inspection of the curves reveals that a peak value of D_r is observed and then D_r decreases with increasing A^+T^+.

To understand the effect of spanwise wall oscillations in detail, we consider an interrelated length scale with the wall oscillation. In Eq. (4), the wall oscillation decays exponentially from the wall. When threshold value W_t^+ is set, the depth of the Stokes layer penetrating into the internal flow is defined as

$$y_d^+ = \sqrt{T^+/\pi}\, \ln\left(A^+ \Big/ W_t^+\right) \tag{5}$$

where y_d^+ represents a thickness within the influence of the Stokes layer. Note that this is different from the Stokes layer thickness $\delta^+ = \sqrt{(4\pi T^+)}$, where the influence of A^+ is not included. It is known that the maximum root mean squared value of spanwise turbulent velocity fluctuations near the wall is about $w_{\text{rms}}^+ \simeq 1.0$. To give an influence on drag reduction by the spanwise oscillations, the threshold value of W_t^+ should be set within the maximum value of w_{rms}^+. Accordingly, the threshold value is set as $W_t^+ = 0.5$ in the present study.

The role of y_d^+ on drag reduction is analyzed by examining the interrelation between streamwise vortices and near-wall low- and high-speed streaks. The streamwise vortices are represented by a contour of the positive second invariant of the velocity gradient tensor,[13] which is defined as

$$Q = \tfrac{1}{2}\left(\Omega_{ij}^2 - S_{ij}^2\right) \tag{6}$$

where S_{ij} is the tensor of strain rate and Ω_{ij} is the tensor of rotation. Note that $Q > 0$ indicates the existence of streamwise vortices near the wall. In the first place, the interrelation is inspected at $y^+ = 10$. The flow fields are conditionally averaged in the x and θ directions for $Q > 1$ and $\omega_x > 0$. This procedure is performed in a stationary turbulent pipe flow at $Re_m = 4.9 \times 10^3$ ($Re_\tau = 1.7 \times 10^2$), and the results are shown in Fig. 3a. Here, $\omega_x > 0$ represents that the streamwise vortices rotate in the counterclockwise direction. As seen in Fig. 3a, a streamwise vortex is located in between the low-and high-speed streaks. The streamwise vortex makes the high-speed fluid ($u' > 0$) move toward the wall and the low-speed fluid ($u' < 0$) move away from the wall. This contributes to the generation of Reynolds shear stress $\overline{u'v'}$ (Ref. 2). When the conditional averaging is taken at $Q > 1$ and $\omega_x < 0$ in Fig. 3b, the flow structure is almost the same as that in Fig. 3a with the opposite direction. Accordingly, the case of $\omega_x > 0$ is chosen and dealt with in the present analysis.

When the spanwise wall oscillation is imposed, the interaction between streamwise vortices and streak structures is scrutinized in detail. As mentioned earlier, the selection of y_d^+ is important in the analysis of drag reduction. To examine the direct influence of

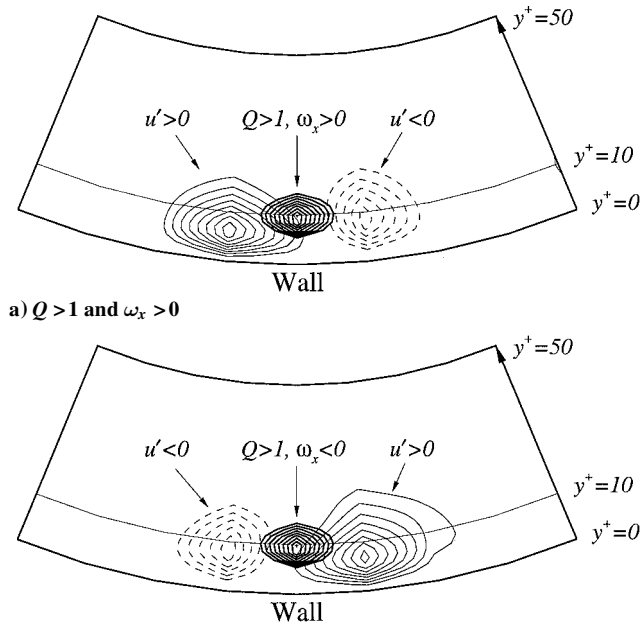

Fig. 3 Conditionally averaged flowfield associated with streamwise vortices at $y^+ = 10$.

the wall oscillation on the interactions, sequential pictures of the conditionally phase-averaged flow structures at $y^+ = 10$ for one wall oscillation cycle are displayed in Fig. 4. Two cases in Table 2 are employed: $y_d^+ = 14.3$ in case 1 and $y_d^+ = 22.7$ in case 2. Because the conditional averaging is taken at $y^+ = 10$, the flow structures of two cases are fully embedded in the aforestated Stokes layer. As shown in Fig. 4, at $\pi/4$, both the wall and the streamwise vortex rotate in the counterclockwise direction. In the near-wall region, the high-speed (solid line) and low-speed (dotted line) fluids are driven to move to the right by both the rotations of the wall and the streamwise vortex. The high-speed fluid intrudes beneath the low-speed fluid. At $\pi/2$, the velocity of the wall achieves its maximum value, and the intrusion of the high-speed fluid is also augmented. Around the streamwise vortex, the gradient of u' in the wall-normal direction is increased. At $3\pi/4$ and π, the speed of the wall is decreased, and the intrusion of the high-speed fluid is relatively weakened.

During the decelerating phase ($5\pi/4$), the wall rotates in the clockwise direction, which causes the near-wall high-speed fluid to move to the left. At $3\pi/2$, the wall speed gets its maximum value, and the high-speed fluid extends farther to the left. Because the streamwise vortex rotates in the counterclockwise direction, its rotation counteracts the effect of the clockwise motion of the wall. As seen in Fig. 4, the low-speed fluid is almost lessened. In addition, the location of the low-speed fluid around the vortex is not as close to the wall as the high-speed fluid. Hence, the influence of the wall movement on the low-speed fluid is greatly reduced. Because of these two effects, the low-speed fluid can hardly intrude beneath the high-speed fluid. At the phases of $7\pi/4$ and 2π, the speed of

Table 2 Three cases of the present analysis

Case	A^+	T^+	y_d^+	a_5^+	V_c^+	D_r
1	5.3	115.7	14.3	0.126	0.120	24.1
2	10.6	173.5	22.7	0.196	0.147	35.3
3	13.2	115.7	19.9	0.314	0.167	39.7

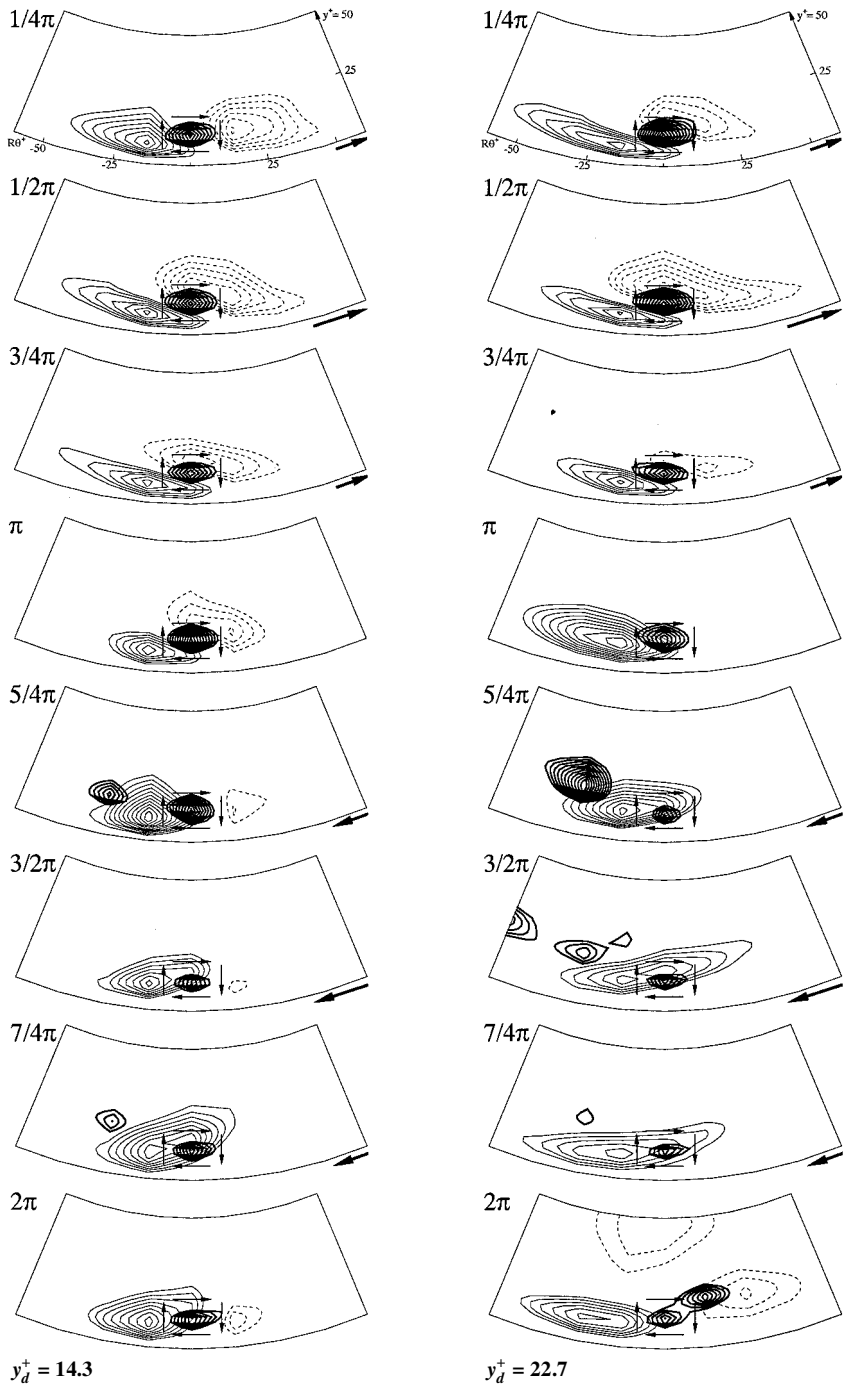

Fig. 4 Conditionally averaged flow structures at $y^+ = 10$.

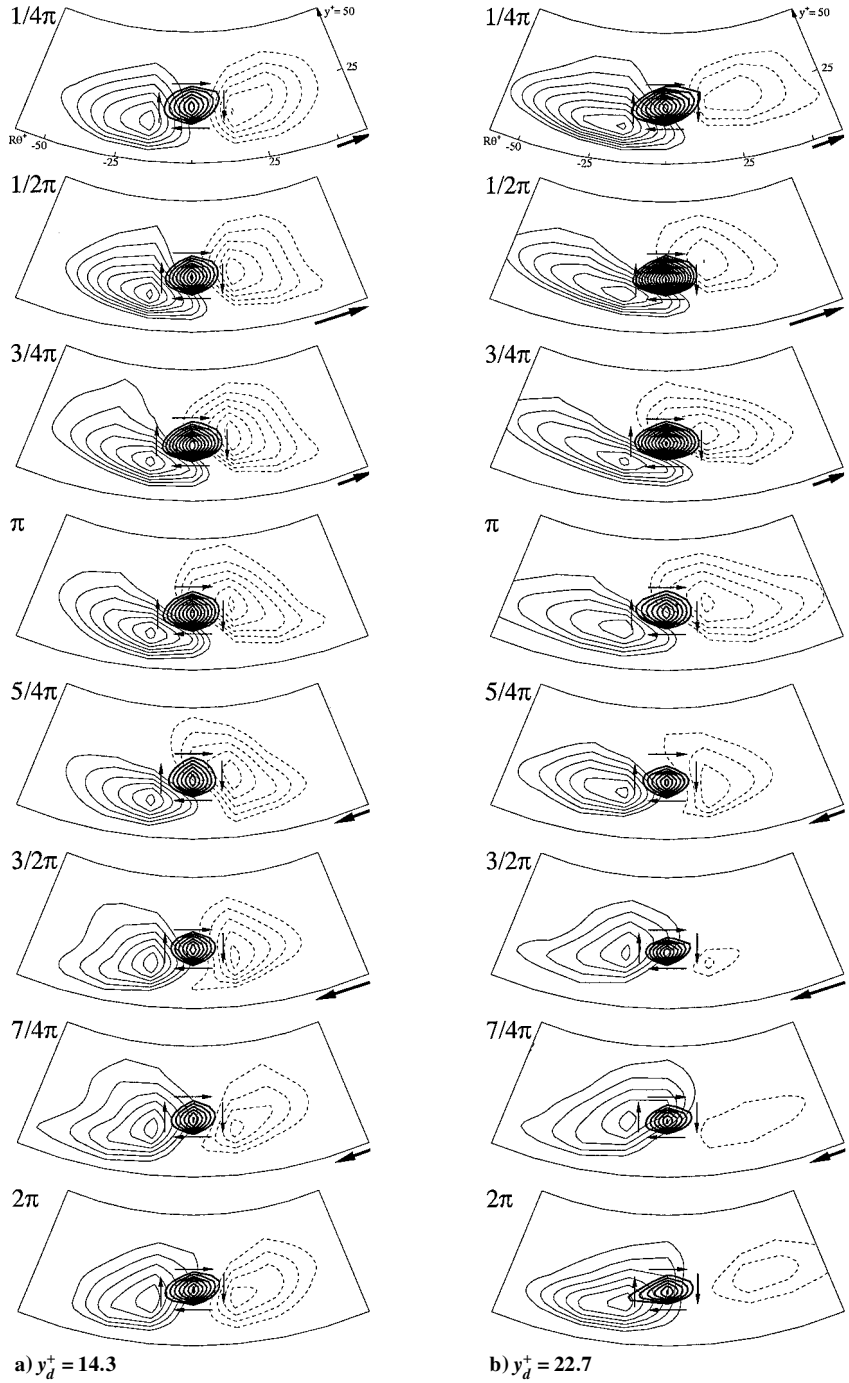

Fig. 5 Conditionally averaged flow structures at $y^+ = 20$.

the wall is decreased, and the right extension of the high-speed fluid is shrunk. The streamwise vortex is mainly surrounded by the high-speed fluid. The sequential illustrations in Fig. 4 clearly show the response of vortex-associated flowfields to the oscillation of the wall. Quadrio and Sibilla[8] suggested a conceptual model, which is consistent with the present description of the scenario in the first half of the oscillation period.

Next, the conditionally averaged flowfields at $y^+ = 20$ are illustrated in Fig. 5. As employed in Fig. 4, the same two cases are adopted for comparison. Because the conditional averaging is taken at $y^+ = 20$, case 2 ($y_d^+ = 22.7$) is fully embedded in the aforestated Stokes layer, whereas case 1 ($y_d^+ = 14.3$) is not. For case 1, the streamwise vortices at $y^+ = 20$ are out of the influence range of the Stokes layer. Accordingly, the flowfields are not substantially changed. In case 2, however, the flowfields are still in the influence range of the Stokes layer. A closer inspection of the flowfields in Fig. 5b indicates that the high-speed fluid intrudes beneath the low-speed fluid in the first-half of the oscillating period ($0 \le t/T \le \pi$). In the second half of the oscillating period ($\pi \le t/T \le 2\pi$), the streamwise vortex is mainly surrounded by the high-speed fluid. However, the intrusion of the high-speed fluid in Fig. 5a is not active as compared to the case in Fig. 6b. Furthermore, the low-speed fluid is not disturbed by the oscillations. The flow pattern in Fig. 5a is very similar to that in Fig. 6, where the wall is stationary. When the flow structures in Figs. 4 and 5 are summarized, a conclusion emerges that the streamwise vortices within the depth of penetration of the Stokes layer (y_d^+) are influenced by the spanwise oscillations.

By the utilization of y_d^+, the drag reduction rate is plotted in Fig. 7. As anticipated, D_r increases with increasing y_d^+. However, several exceptional cases still exist, in which D_r increases to a certain value and then decreases with the increase of y_d^+. These exceptional cases imply that the rate of drag reduction is not only governed by the influence range of the Stokes layer. There exist other factors that affect the drag reduction rate. If the wall continues to move in the spanwise direction with a constant speed, the turbulence in the vicinity of the wall is also readjusted. However, the amount of drag

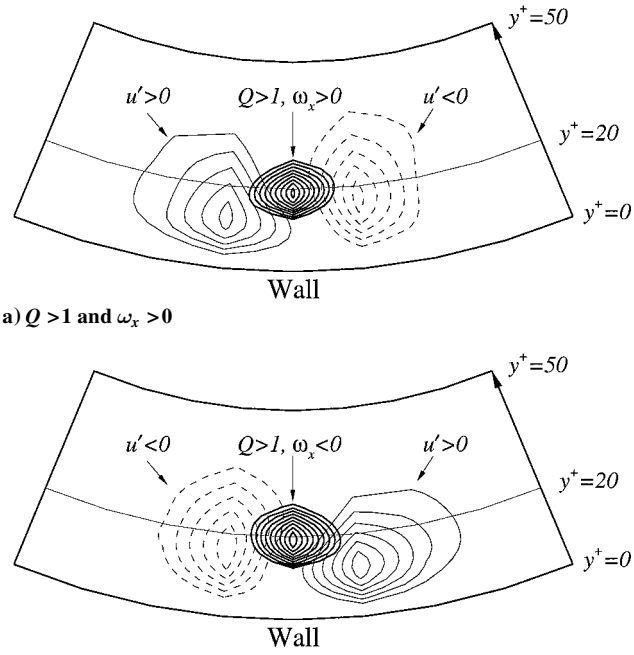

a) $Q > 1$ and $\omega_x > 0$

b) $Q > 1$ and $\omega_x < 0$

Fig. 6 Conditionally averaged flowfield associated with streamwise vortices at $y^+ = 20$.

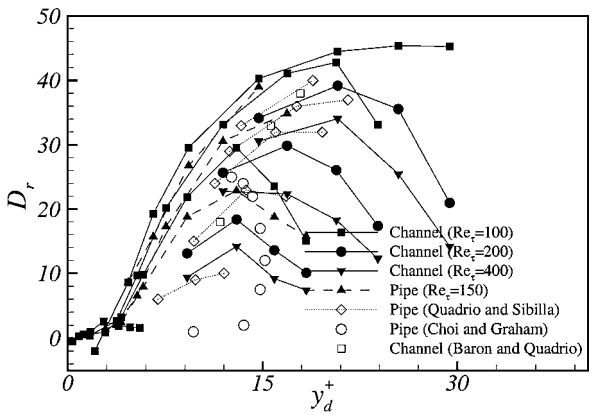

Fig. 7 Drag reduction rate as a function of y_d^+.

reduction achieved in a steadily rotating pipe is not as much as that in a pipe that oscillates around its axis sinusoidally.[8,14] The only difference between the oscillating motion and the steadily rotating motion is that an acceleration exists in the oscillating motions. This difference gives us an acceleration parameter in the Stokes layer as a measure of the amount of drag reduction. From the dynamic point of view, acceleration represents an inertial force of fluid in unit mass, which is a measure of the change of the relative position between fluid elements by the Stokes layer.

To examine the effect of acceleration in the present spanwise wall oscillations, the skewness and flatness are computed and displayed in Fig. 8. Two cases are chosen in Table 2: One is case 1 for a lower acceleration, and the other is case 3 for a higher acceleration. The case of no control is also included for comparison. As shown in Fig. 8a, when the spanwise wall oscillation is imposed, the skewness is augmented, and the maximum of the skewness moves apart from the wall. In the buffer layer ($15 \leq y^+ \leq 30$), the skewness of the spanwise oscillations is positive whereas the skewness of no control is negative. This means that the high-speed fluid by the wall oscillation is skewed as compared to that of no control. As addressed by Quadrio and Sibilla,[8] the elongated low-speed streaks are reduced by the spanwise oscillation, whereas some high-speed streaks are enhanced. Accordingly, the skewness is increased by the spanwise oscillation. In Fig. 8a, the skewness of case 3 is higher than that of case 1. As mentioned earlier, the acceleration of case 3 is larger

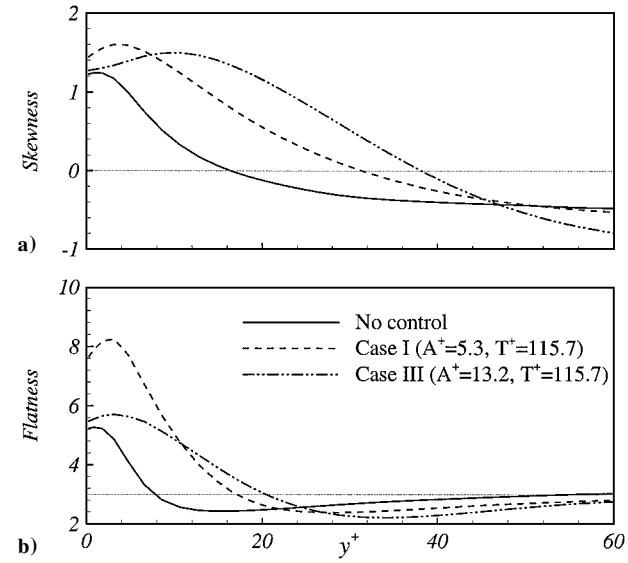

Fig. 8 Skewness and flatness of streamwise velocity fluctuations.

than that of case 1 in the region of $y^+ \geq 8$. This suggests that the higher acceleration enlarges the area of the positive skewness. The flatness in Fig. 8b shows a significant increase in the viscous sublayer region by the oscillation. This may be caused by the increase of intermittency by the oscillation. The maximum flatness is located at $y^+ \simeq 5$, where the flow change in turbulence is highly amplified by the wall oscillation.

Comparison is extended to the probability density function (PDF) of the streamwise velocity fluctuations (u'/u_{rms}) with wall oscillation. In the viscous sublayer region (Figs. 9a and 9b), the PDFs of the negative streamwise velocity fluctuations with spanwise oscillation return back to the center, whereas those of no control are tilted to the negative direction. This may be attributed to the reduction of the elongated low-speed streaks, as stated in Fig. 8a. However, note that the present result is contradictory to the experimental result of Choi and Clayton.[15] The increase of the skewness in this region is directly linked with the shrinkage of the negative PDF. This is also consistent with the result of Quadrio and Sibilla.[8] As the acceleration increases, that is, in case 3, the maximum location of PDF moves to the center. This shows a tendency to isotropy due to acceleration. A closer inspection of the positive PDFs in the long-tail region ($2 \leq u'/u_{\text{rms}} \leq 4$) in Figs. 9b and 9c discloses that the PDF distributions are intercrossed because the detection layer is far from the wall. Close-up views of the PDF in the insets indicate that the PDFs of cases 1 and 3 are larger than that of no control in Fig. 9c. The increase in the long-tail region may be related to the high-speed streaks by the wall oscillations.[15] Because the detection layer is apart from the wall ($y^+ > 20.4$), the influence of the wall oscillation is gradually weakened. In the outer region ($y^+ = 50.1$), three PDFs collapse to one curve. A global inspection of Fig. 9 shows that the changes in turbulence statistics in the oscillating boundary layer seem to come mainly from a reduction in the negative probability. Moreover, a significant change of the positive PDF distribution in the long-tail region occurs in the viscous sublayer region close to approximately $y^+ \simeq 5$.

Now, the influence of the acceleration in the Stokes layer is implemented in the present formulation of the drag reduction rate D_r. According to Eq. (4), the acceleration of the Stokes layer is derived as

$$a^+ = 2\pi (A^+/T^+) \exp\left[-\sqrt{(\pi/T^+)}\, y^+\right] \tag{7}$$

where a critical value of a^+ is chosen at $y^+ = 5$ in the present study. The main rationale for the selection a_5^+ is that the flatness in Fig. 8 has a maximum at $y^+ \simeq 5$. Furthermore, the change of the PDF in Fig. 9 is significant at around $y^+ \simeq 5$. In Fig. 10, D_r is plotted as a function of a_5^+. As a_5^+ increases, D_r increases on the surface. However, some inflection points are displayed. After passing the inflection points, D_r increases with decreasing a_5^+. The exceptional

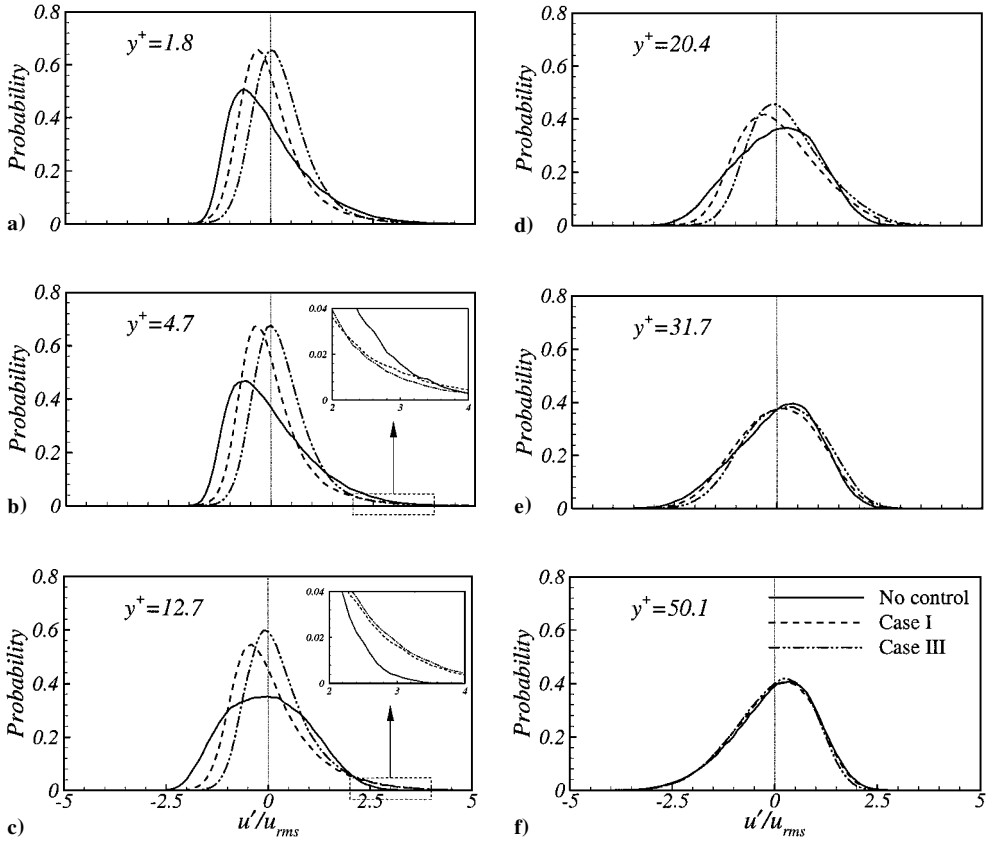

Fig. 9 Comparison of the PDFs near the wall.

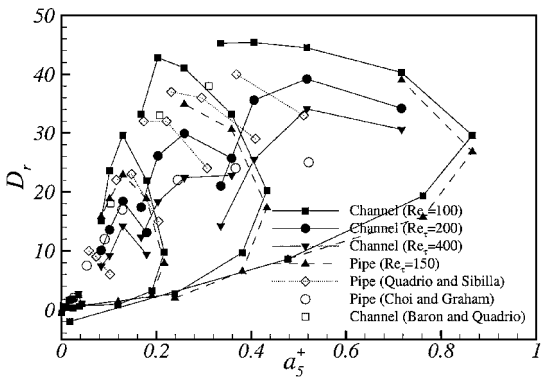

Fig. 10 Drag reduction rate as a function of a_5^+.

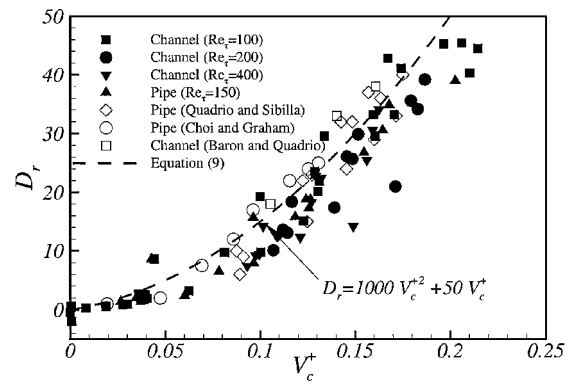

Fig. 11 Drag reduction rate as a function of $V_c^+ = y_d^+ a_5^+/(A^+ Re^{0.2})$.

cases in Fig. 7 may be related to the inflection points in Fig. 10. Two curves in Figs. 7 and 10 suggest that two parameters, y_d^+ and a_5^+, should be combined together to make a better similarity of D_r. Because y_d^+ represents the influence range of the Stokes layer, and a_5^+ is a measure of the acceleration of the Stokes layer, a combined parameter V_c^+ is proposed:

$$V_c^+ = \left(a_5^+ y_d^+ \Big/ A^+ Re_\tau^{0.2}\right) \tag{8}$$

where the Reynolds number effect is also included. If the Reynolds number effect is neglected, the data scattering is more intensified. When V_c^+ is employed, a good correlation equation is obtained as shown in Fig. 11:

$$D_r = 1000 V_c^{+2} + 50 V_c^+ \tag{9}$$

As seen in Fig. 11, all of the available data collapse well in Eq. (9).

The response of near-wall turbulence to the wall oscillations can be quantitatively represented by the changes in turbulence statistics. In the first half of the oscillation period, the intrusion of the high-speed fluid beneath the low-speed fluid gives the increase of $\partial u'/\partial y$. It is known that the change of $\partial u'/\partial y$ is reflected in the change of the wall-normal vorticity fluctuations ω_θ' (Ref. 8). The change of the relative position between streamwise vortex and low- and high-speed fluids can greatly influence the generation of Reynolds shear stress $\overline{u'v'}$. The distributions of $\overline{u'v'}$ along the y^+ direction are displayed in Fig. 12 for different cases. Note that $\overline{u'v'}$ is directly correlated with V_c^+, that is, $\overline{u'v'}$ decreases with increasing V_c^+. However, the discrepancy between case 1 and case 2 is unclear.

The influence of V_c^+ on the quadrants of $\overline{u'v'}$ is displayed in Fig. 13. The high-speed fluid component in the quadrants $\langle\overline{u'v'}\rangle_{\mathrm{I}}$ and $\langle\overline{u'v'}\rangle_{\mathrm{IV}}$ are shown in Fig. 13a, whereas the low-speed fluid component in the quadrants $\langle\overline{u'v'}\rangle_{\mathrm{II}}$ and $\langle\overline{u'v'}\rangle_{\mathrm{III}}$ are in Fig. 13b. When the spanwise oscillation is not imposed, that is, no control, it is shown that the contributions of $\langle\overline{u'v'}\rangle_{\mathrm{I}}$ and $\langle\overline{u'v'}\rangle_{\mathrm{III}}$ to $\overline{u'v'}$ are smaller than those of $\langle\overline{u'v'}\rangle_{\mathrm{II}}$ and $\langle\overline{u'v'}\rangle_{\mathrm{IV}}$. When the spanwise oscillation is imposed, the contributions of $\langle\overline{u'v'}\rangle_{\mathrm{I}}$ and $\langle\overline{u'v'}\rangle_{\mathrm{IV}}$ are significant as compared to those of $\langle\overline{u'v'}\rangle_{\mathrm{II}}$ and $\langle\overline{u'v'}\rangle_{\mathrm{III}}$. In particular,

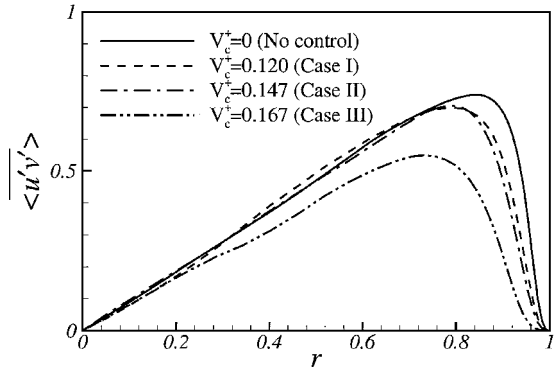

Fig. 12 Influence of V_c^+ on $\overline{u'v'}$.

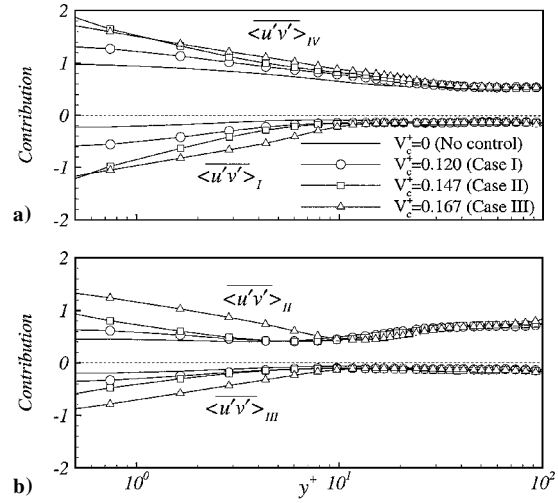

Fig. 13 Influence of V_c^+ on the quadrants of $\overline{u'v'}$.

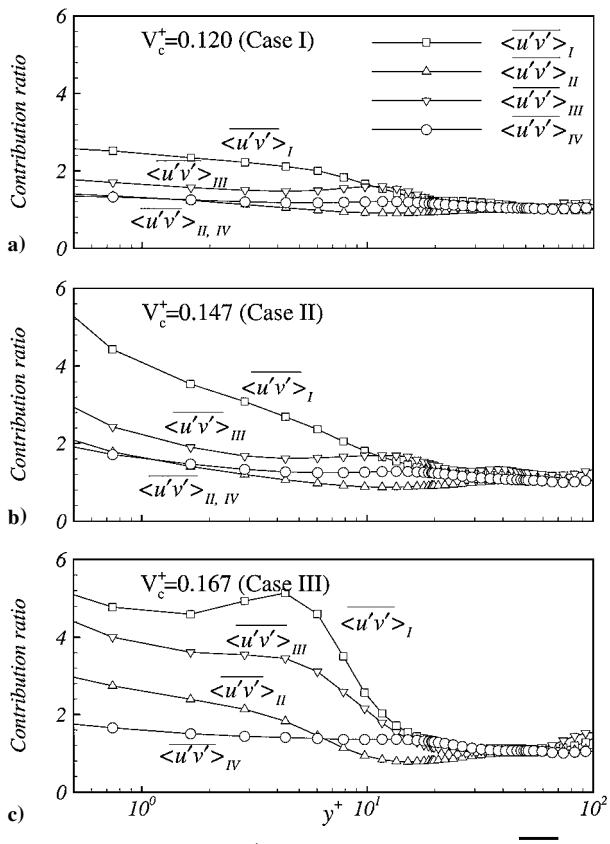

Fig. 14 Influence of V_c^+ on the contribution ratio of $\overline{u'v'}$.

as V_c^+ increases, the role of $\langle\overline{u'v'}\rangle_{\mathrm{I}}$ on $\overline{u'v'}$ is enhanced. This may be attributed to the ejection of the high-speed fluid near the wall. To see the influence of V_c^+ on the quadrants of $\overline{u'v'}$ in detail, a contribution ratio is defined as

$$\text{contribution ratio} = \frac{(\text{quadrant of } \overline{u'v'})_{\text{control}}}{(\text{quadrant of } \overline{u'v'})_{\text{no control}}} \tag{10}$$

where the quadrants of $\overline{u'v'}$ in the spanwise oscillations are normalized by the corresponding quadrants of no control. The contribution ratios in the vicinity of the wall are exhibited in Fig. 14, where the contribution of $\langle\overline{u'v'}\rangle_{\mathrm{I}}$ is outstanding. Furthermore, as V_c^+ increases, the contribution of $\langle\overline{u'v'}\rangle_{\mathrm{I}}$ is amplified. As mentioned earlier, the ejection of the high-speed fluid plays an important role on the attenuation of $\overline{u'v'}$ near the wall. The increase in V_c^+ activates the contribution of $\langle\overline{u'v'}\rangle_{\mathrm{I}}$.

Conclusions

Detailed numerical simulations have been performed to elucidate the drag reduction by spanwise wall oscillations in turbulent channel and pipe flows. To extract a simple equation for expressing the drag reduction rate D_r, several parameters have been employed, for example, A^+, T^+, and A^+T^+. Based on the interaction between the Stokes layer and near-wall turbulence when wall oscillations are present, a new parameter $V_c^+ = a_5^+ y_d^+/(A^+ Re_\tau^{0.2})$ was proposed. Here, y_d^+ represents the influence range of the Stokes layer, and a_5^+ is a measure of the acceleration of the Stokes layer at $y^+ = 5$. By the use of this parameter, the drag reduction rate showed a good correlation curve. To understand the drag reduction mechanism and to show the physical grounds for the selection of V_c^+, the interrelation between streamwise vortices and near-wall low- and high-speed streaks was scrutinized in detail by examining conditionally averaged DNS results. Examination of the results indicated that the relations between streamwise vortices and high- and low-speed fluids are greatly affected within the influence range of the Stokes layer. The high-speed fluid intrudes beneath the low-speed fluid in the first half of the oscillating period. In the second half of the oscillating period, the streamwise vortex is mainly surrounded by the high-speed fluid and the low-speed fluid is almost lessened. When the streamwise vortices are out of y_d^+, the relative position between streamwise vortices and high- and low-speed fluids is similar to that in a flow with stationary wall. The changes of $\overline{u'v'}$ were examined for several oscillating conditions. This was because the turbulent friction drag is closely related to the level of $\overline{u'v'}$. The quadrant analysis of $\overline{u'v'}$ indicated that the contribution of V_c^+ to $\langle\overline{u'v'}\rangle_{\mathrm{I}}$ is dominant.

Acknowledgments

This research was supported by a grant from the National Research Laboratory of the Ministry of Science and Technology, Republic of Korea. The first author acknowledges the support of the Korea Science and Engineering Foundation and the National Science Foundation of China (Grants 10072032 and 19732005).

References

[1]Robinson, S. K., "The Kinematics of Turbulent Boundary Layer Structure," Ph.D. Dissertation, Dept. of Mechanical Engineering, Stanford Univ., Stanford, CA, March 1991.

[2]Kim, J., Moin, P., and Moser, R. K., "Turbulence Statistics in Fully Developed Channel Flow at Low Reynolds Number," *Journal of Fluid Mechanics*, Vol. 177, 1987, pp. 133–166.

[3]Jung, W. J., Mangiavacci, N., and Akhavan, R., "Suppression of Turbulence in Wall-Bounded Flows by High-Frequency Spanwise Oscillations," *Physics of Fluids*, Vol. 4, No. 8, 1992, pp. 1605–1607.

[4]Laadhari, F., Skandaji, L., and Morel, R., "Turbulence Reduction in a Boundary Layer by a Local Spanwise Oscillating Surface," *Physics of Fluids*, Vol. 6, No. 10, 1994, pp. 3218–3220.

[5]Choi, K.-S., DeBisschop, J. R., and Clayton, B. R., "Turbulence Boundary Layer-Control by Means of Spanwise-Wall Oscillation," *AIAA Journal*, Vol. 36, No. 7, 1998, pp. 1157–1163.

[6]Baron, A., and Quadrio, M., "Turbulent Drag Reduction by Spanwise Wall Oscillation," *Applied Scientific Research*, Vol. 55, 1996, pp. 311–326.

[7]Choi, K. S., and Graham, M., "Drag Reduction of Turbulent Pipe Flows by Circular-Wall Oscillation," *Physics of Fluids*, Vol. 10, No. 1, 1998, pp. 7–9.

[8]Quadrio, M., and Sibilla, S., "Numerical Simulation of Turbulent Flow in a Pipe Oscillating Around Its Axis," *Journal of Fluid Mechanics*, Vol. 424, 2000, pp. 217–241.

[9]Schlichting, H., *Boundary-Layer Theory*, McGraw–Hill, NewYork, 1968, pp. 93–95.

[10]Ma, B., Von Doorne, C. W. H., Zhang, Z., and Nieuwstadt, F. T. M., "On the Spatial Evolution of a Wall-Imposed Periodic Disturbance in Pipe Poiseuille Flow at $Re = 3000$. Part 1. Subcritical Disturbances," *Journal of Fluid Mechanics*, Vol. 398, 1999, pp. 181–224.

[11]Karniadakis, G. E., Israeli, M., and Orszag, S. A., "High-Order Splitting Methods for the Incompressible Navier–Stokes Equations," *Journal of Computational Physics*, Vol. 97, 1991, pp. 414–443.

[12]Orlandi, P., and Jimenez, J., "On the Generation of Turbulent Wall Friction," *Physics of Fluids*, Vol. 6, No. 2, 1994, pp. 634–641.

[13]Cucitore, R., Quadrio, M., and Baron, A., "On the Effectiveness and Limitations of Local Criteria for the Identification of a Vortex," *European Journal of Mechanics B/Fluids*, Vol. 18, 1999, pp. 261–282.

[14]Orlandi, P., and Fatica, M., "Direct Simulations of Turbulent Flow in a Pipe Rotating About Its Axis," *Journal of Fluid Mechanics*, Vol. 343, 1997, pp. 43–72.

[15]Choi, K.-S., and Clayton, B. R., "The Mechanism of Turbulent Drag Reduction with Wall Oscillation," *International Journal of Heat and Fluid Flow*, Vol. 22, 2001, pp. 1–9.

R. M. C. So
Associate Editor